Kovove Mater. 59 2021 279–289
DOI: 10.4149/km_2021_5_279

The transition from the power-law to the power-law breakdown regimes in thermal creep of Zr1%Nb cladding alloys

V. Sklenicka[1,2]*, K. Kucharova[1], M. Kvapilova[1,2], P. Kral[1,2], J. Dvorak[1,2]

[1] *Institute of Physics of Materials, Czech Academy of Sciences, 616 62 Brno, Czech Republic*
[2] *Central European Research Institute of Technology – IPM CZ, 616 62 Brno, Czech Republic*

Received 16 August 2021, received in revised form 30 August 2021, accepted 7 September 2021

Abstract

In the present study, the tensile creep behaviour of three various cladding tubes of the Zr1%Nb alloy has been studied in the α-Zr region at 350 °C, which corresponds to the operational service conditions of the cladding tubes in nuclear light-water reactors. Tensile creep tests under the high constant applied stress region from 150 to 260 MPa have been carried out at the transition from the power-law (PL) to the power-law breakdown (PLB) regimes. It was found that all dispersion strengthened Zr1%Nb cladding alloys under investigation reach the PLB regime at values of the compensated applied stress σ/G above approximately 8×10^{-3}, where the stress exponent n of the minimum creep rate $\dot{\varepsilon}_{\mathrm{m}}$ ($n = (\partial \ln \dot{\varepsilon}_{\mathrm{m}}/\partial \ln \sigma)_{\mathrm{T}}$) then dramatically increases from the value of ~ 6 with increasing stress ratio σ/G. The fact that all experimental results for both the PL and PLB obey the Monkman-Grant relationship supports the idea that the creep mechanism in the PL and PLB does not change qualitatively and indicates a close link between the deformation and fracture processes in both creep regimes under investigation. However, future experiments could be carried out at different testing temperatures within the PLB regime to verify the controversial contemporary views.

K e y w o r d s: zirconium alloy, creep testing, power-law breakdown, creep mechanisms, fracture

1. Introduction

Zirconium Zr1%Nb (E110) alloy and its modified versions with optimized compositions are used as fuel cladding tubes in nuclear light-water VVER-type reactors [1]. Since the tubes are exposed to high pressure and temperature conditions, creep is a crucial concern for their applications. Cumulative α-zirconium creep data were analysed based on an extensive literature review [2]. However, a complete understanding of the creep deformation and fracture mechanisms operating in a Zr1%Nb alloy is still missing [3–5]. Despite the important basic understanding of creep behaviour in zirconium alloys, there appears to be insufficient creep data in the literature describing the thermal creep in the transition between the power-law (PL) creep regime at moderate applied stresses controlled by dislocation climb and the power-law breakdown (PLB) regime at high stresses [2, 6, 7]. In fact, the mechanism of creep deformation in the PLB is poorly understood due to a limited number of studies carried out in this regime. However, further study of the PLB in zirconium alloys is strongly needed for the safe management of claddings. This was the reason for undertaking the present study, to provide further information on the transition between the PL and the PLB regimes in creep of Zr1%Nb cladding alloys at a temperature of 350 °C matching an operational temperature of cladding materials in the reactor.

2. Experimental

While the zirconium E110 alloy was produced based on electrolytic zirconium, the E110G and the E110E alloys were produced on a sponge basis with a reduced impurity level. The nominal chemical compositions of the tested alloys are shown in Table 1.

*Corresponding author: e-mail address: sklen@ipm.cz

Table 1. Chemical composition of zirconium alloys under investigation

Alloy	Nb	Fe	H	N	C	O	Hf	F	Si	Ca
	(wt.%)	(ppm)							(wt.%)	
E110	1.07 ± 0.1		10 ± 5	25 ± 5	max 100	400 ± 100	500	–	–	–
E110G	1.1	550	10	30	100	1000	100		< 0.01	< 0.01
E110E	1.01	500	3	30	50	710	–	< 1	–	–

Specimens of cladding tubes in the as-received conditions (80 mm in length, 9.13 mm in outer diameter, and 0.7 mm in wall thickness) were used. Creep specimens with a gauge length of 50 mm were manufactured from the original cladding tubes. Uniaxial constant stress creep tests in tension were carried out in an argon atmosphere [3]. The creep testing was conducted at 350 ℃ (a typical operating temperature in VVER--type reactors), with the testing temperature maintained to within ± 0.5 ℃. The applied tensile stresses σ ranged from 150 to 260 MPa. The creep elongations were measured using a linear variable differential transducer (LVDT) with a sensitivity of 5×10^{-6}, and they were continuously recorded digitally, and computer processed. The minimum creep rates, $\dot{\varepsilon}_{\mathrm{m}}$, were determined using modified creep curves of strain rate $\dot{\varepsilon}$ vs time t [8]. The microstructural and fractographic investigations were performed using a Tescan Lyra 3 scanning electron microscope (SEM). The EBSD data were analysed using HKL Channel 5 software (Oxford Instruments, UK). The dislocation substructure was investigated using a transmission electron microscope (TEM) Jeol 2100F operating at 200 kV. Details of the microstructural and fractographic methods used can be found in our earlier paper [8].

3. Results and discussion

A detailed microstructural investigation of the Zr1%Nb alloy before and after creep exposure has been reported in our previous study [8]. At 350 ℃, two kinds of precipitates of secondary phases (the β-(Zr,Nb) precipitates and the minor Laves phase $Zr(Nb,Fe)_2$ were identified, which were homogeneously located intragranularly and intergranularly in the α-Zr matrix. Accordingly, the solid solution strengthening effect of niobium is increased by the synergistic action of the precipitation strengthening effect of the secondary phases in the creep of the studied alloys.

3.1. Stress dependence of the minimum creep rate $\dot{\varepsilon}_{\mathrm{m}}$

The minimum creep rate, $\dot{\varepsilon}_{\mathrm{m}}$, is a function of temperature T and applied stress σ:

$$\dot{\varepsilon}_{\mathrm{m}} = \dot{\varepsilon}_{\mathrm{m}}(T, \sigma) . \tag{1}$$

In the interval of moderate stresses and at a constant temperature corresponding to the power-law (dislocation) regime [2, 3, 6, 8], the semi-empirical relationship

$$\dot{\varepsilon}_{\mathrm{m}} = A\sigma^n \tag{2}$$

is frequently applied to describe the stress dependence of the minimum creep rate $\dot{\varepsilon}_{\mathrm{m}}$. In Eq. (2), A is a dimensionless and material-dependent constant at a given temperature. The stress exponent of the minimum creep rate, n, is then defined as

$$n = (\partial \ln \dot{\varepsilon}_{\mathrm{m}} / \partial \ln \sigma)_{\mathrm{T}} . \tag{3}$$

At very high stresses corresponding to the power-law breakdown and/or exponential creep regime [2, 3, 6, 8, 9], the stress dependence of the minimum creep, $\dot{\varepsilon}_{\mathrm{m}}$, is described by an empirical relationship:

$$\dot{\varepsilon}_{\mathrm{m}} = A' \exp(B\sigma) , \tag{4}$$

where A' and B are constants. As proposed by Garofalo [10], both the power-law and exponential stress regimes relationships can be put together into a single relationship

$$\dot{\varepsilon}_{\mathrm{m}} = A'' (\sinh B'\sigma)^n . \tag{5}$$

This relationship reduces to Eq. (2), in which $A = (B')^n A''$ at low stresses, and to Eq. (4), in which $A' = A''$ and $B = nB'$ at high stresses.

The stress dependences of the minimum creep rate, $\dot{\varepsilon}_{\mathrm{m}}$, for the cladding alloys under investigation are shown in Fig. 1a in double logarithmic plots. Based on our preliminary results [8], the values of the applied stress, σ, were chosen in such a way that the minimum creep rates within the range of $10^{-8}\,\mathrm{s}^{-1}$ to $10^{-2}\,\mathrm{s}^{-1}$ had been expected to cover the desired transition from the power-law to power-law breakdown regimes. Figure 1a shows that the stress dependences are not given by straight lines, which implies that the stress dependences of the minimum creep rates cannot be described by a simple power function with a constant value of the stress exponent n. Actually,

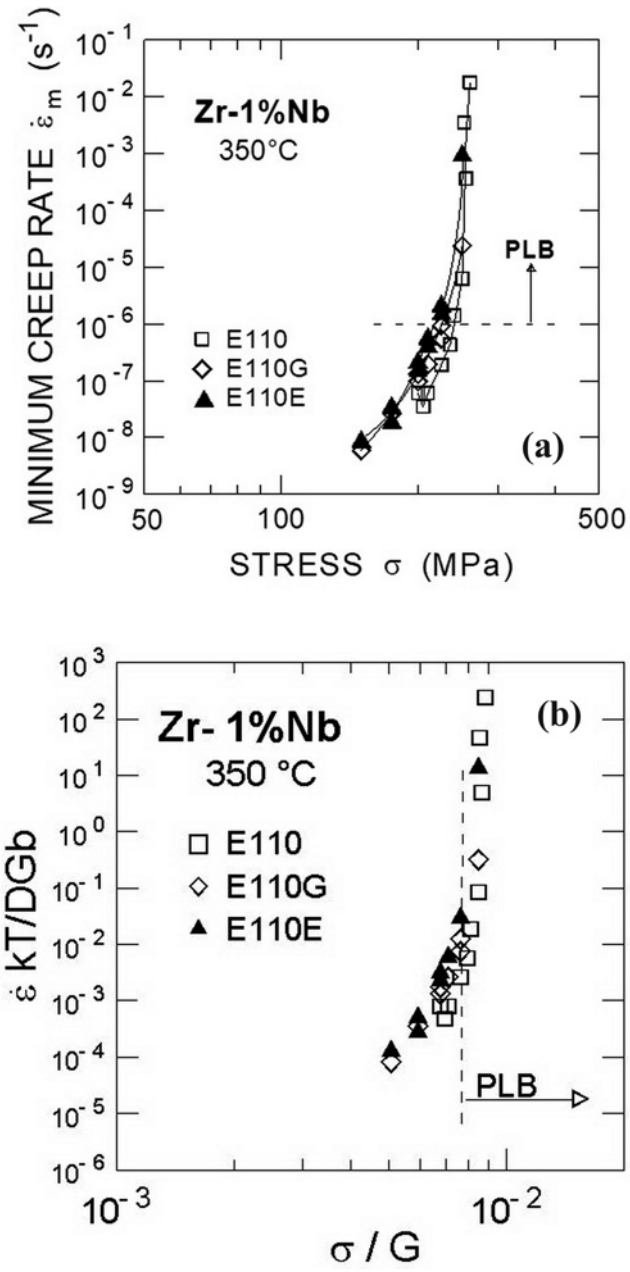

Fig. 1. Dependence of the minimum creep rate $\dot{\varepsilon}_m$ on the applied stress σ: (a) $\dot{\varepsilon}_m$ vs σ, (b) diffusion coefficient-compensated minimum creep rate vs. modulus-compensated applied stress (data for diffusion coefficient D and modulus G were taken from the literature [2, 4]).

the values of the stress exponent n (which are slopes in Fig. 1a), increase with increasing σ from a value of approximately ~ 6 at moderate stresses, which is next to the range of the power-law regime [2–6, 8], to very high values of ~ 65 at the highest stresses, implying the power-law breakdown regime. Although in this work, creep tests have only been carried out at a constant temperature, for mutual comparison with previously reported results [2, 6], a plot of the diffusion coefficient-compensated minimum creep rate, $\dot{\varepsilon}_m$, vs the modulus-compensated applied stress σ/G is shown in Fig. 1b. It is apparent from Fig. 1b that the Zr1%Nb alloys under investigation reach the borderline between the power-law and power-law breakdown regimes at the values of compensated stress σ/G above approximately 8×10^{-3}, where the stress exponent of the minimum creep rate n' then dramatically increases with increasing stress ratio σ/G. Similar σ values of $> 2 \times 10^{-3}G$ and $> 10^{-4}G$ for pure zirconium and Zircaloy alloys, respectively, were reported by Hayes et al. [2] and Kassner et al. [9]. Values of $\sigma > 3 \times 10^{-3}G$ were published by Murty et al. [6].

Such high values of the stress exponent of the minimum creep rate, n, at high applied stresses, σ, are frequently observed in precipitation or dispersion strengthened materials and discontinuously reinforced composites [11]. In this case, one explanation of such extremely high values of n is their rationalization by considering the existence of the effective stress, σ_e, and the threshold stress, σ_0 [11–17], based on the idea that at the highest applied stresses, σ, the creep behaviour is controlled by precipitation strengthening resulting from the mobile dislocations-precipitates interaction, and therefore, the creep behaviour is not driven by the applied stress, σ, but effective stress, σ_e [3, 13–17]. This approach has been widely applied to the creep of precipitation-strengthened alloys. Two different experimental techniques (stress transient dip test technique [18] and strain transient dip test technique [19]) have been proposed for the direct measurement of the effective stress, σ_e [18, 19]. Both techniques rest in determining the reduction of the applied stress σ by $\Delta\sigma = \Delta\sigma_e$. Both these techniques provide very similar results [16]. The relationship between the effective stress, σ_e, and the applied stress, σ, in creep of precipitation strengthened Zr2.5%Nb alloy and pure zirconium based on measuring the effective stress, σ_e, by the modified strain transient dip test technique was reported by Pahutová et al. [3, 20]. However, it should be emphasized that the determination of the effective stress by this method needs a very stress-sensitive technique.

The true stress exponent of the creep rate, n^*, such as the parameter of sensitivity of the minimum creep rate, $\dot{\varepsilon}_m$, to the effective stress, σ_e, can be expressed as

$$n^* = (\partial \ln \dot{\varepsilon}_m / \partial \ln \sigma_e) \tag{6}$$

and

$$\sigma_e = \sigma - \sigma_0, \tag{7}$$

where σ_0 is the threshold stress. If the threshold stress exists, Eq. (2) could be extended for a constant selected testing temperature in such a way that the ef-

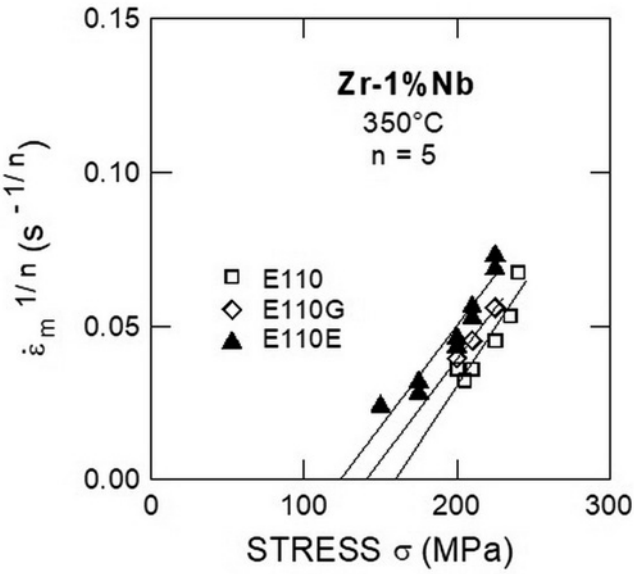

Fig. 2. Estimation of the threshold stress, σ_0, for the stress exponent $n = 5$.

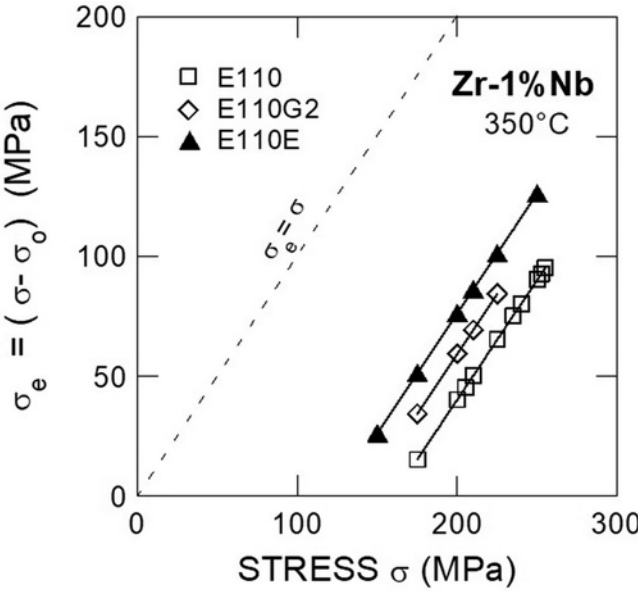

Fig. 3. Relationship between the effective stress, σ_e, and applied stress, σ.

fective stress, σ_e, replaces the applied stress, σ, leading to the relationship

$$\dot{\varepsilon} = A_1 (\sigma - \sigma_0)^{n^*} \tag{8}$$

or

$$\dot{\varepsilon}^{1/n^*} = A_2 (\sigma - \sigma_0) . \tag{9}$$

3.2. The threshold stress σ_0 and effective stress σ_e

Different methods have been proposed to assess the magnitude of the threshold stress, σ_0, in high temperature creep of precipitate and/or dispersion strengthened alloys [11, 21–26]. In this work, the threshold stress was estimated by applying a commonly used linear extrapolation technique [23]. The threshold stress, σ_0, is evaluated graphically for prior selected values of the stress exponent n by plotting $(\dot{\varepsilon}_m)^{1/n}$ vs σ on linear axes, and in the absence of any significant curvature, the plots are extrapolated linearly to intersect the stress axis at zero strain rate. The values of σ_0 of an individual Zr1%Nb alloy were estimated as ~ 160, ~ 141, and ~ 124 MPa for the E110, E110G, and E110E alloys, respectively (Fig. 2). These values of σ_0 are not essentially different from each other. Presupposing that the controlling creep deformation mechanism is dislocation climb and glide, the prior selected value $n = 5$ was used. The estimated values of the threshold stress, σ_0, were used for determining the effective stress, σ_e (Eq. (7)).

The relationship between the effective stress, σ_e, and applied stress, σ, is shown in Fig. 3. From Fig. 3, it can be seen that the effective stress represents a significant fraction of the applied stress, and the σ_e/σ ratio increases with applied stress. For the E110 alloy, the values of the σ_e/σ ratio are ~ 0.25 and ~ 0.4 for 200 and 250 MPa, respectively. Slightly higher values of the σ_e/σ ratio were found for the E110E alloy: ~ 0.38 (200 MPa) and ~ 0.5 (250 MPa). It will be interesting to compare these findings with previously reported results. The measurement of the mean effective stress in creep of pure α-Zr [20] by the strain transient dip test technique led to the conclusion that the effective stress, σ_e, does not depend on the temperature and increases linearly with applied stress, σ. By contrast, the same authors reported [3] that in the case of precipitation strengthened Zr-Nb alloys with different Nb content, the temperature dependence of the effective stress, σ_e, increases with increasing Nb concentration. The values of the σ_e/σ ratio reached as high as 0.5 at high testing temperatures (up to 550 °C) and applied stresses [3].

A question naturally arises about the nature of the threshold stress, σ_0. In principle, the threshold stress is attributed to the presence of the second phase precipitates, which act as obstacles to dislocation motion. The different interpretations of the threshold stress and obstacle strength parameters for particle-strengthened metals have been reviewed by Gibeling [13]. Unfortunately, although the threshold stress phenomenon has been studied in a large number of precipitate-strengthened metallic materials over the past three decades, our present understanding of

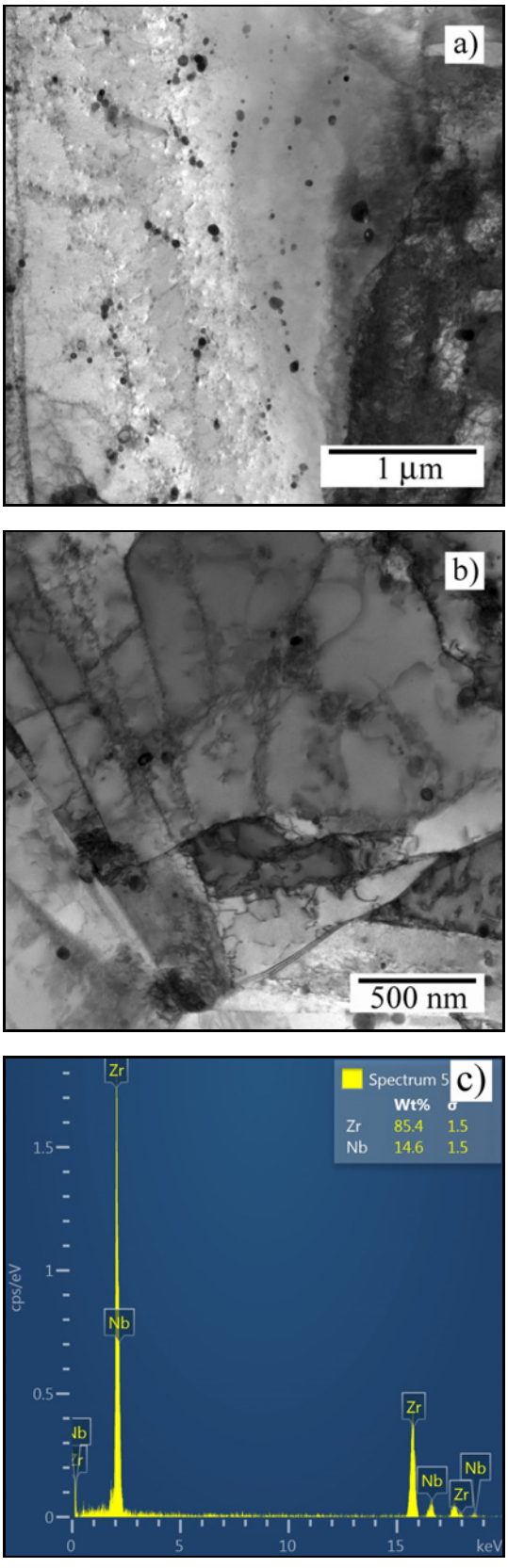

Fig. 4. Nb rich β-Zr precipitates after creep of the Zr1%Nb alloy in the PLB regime: (a), (b) distribution view and (c) EDS spectrum and average composition (creep at 350 °C and 215 MPa).

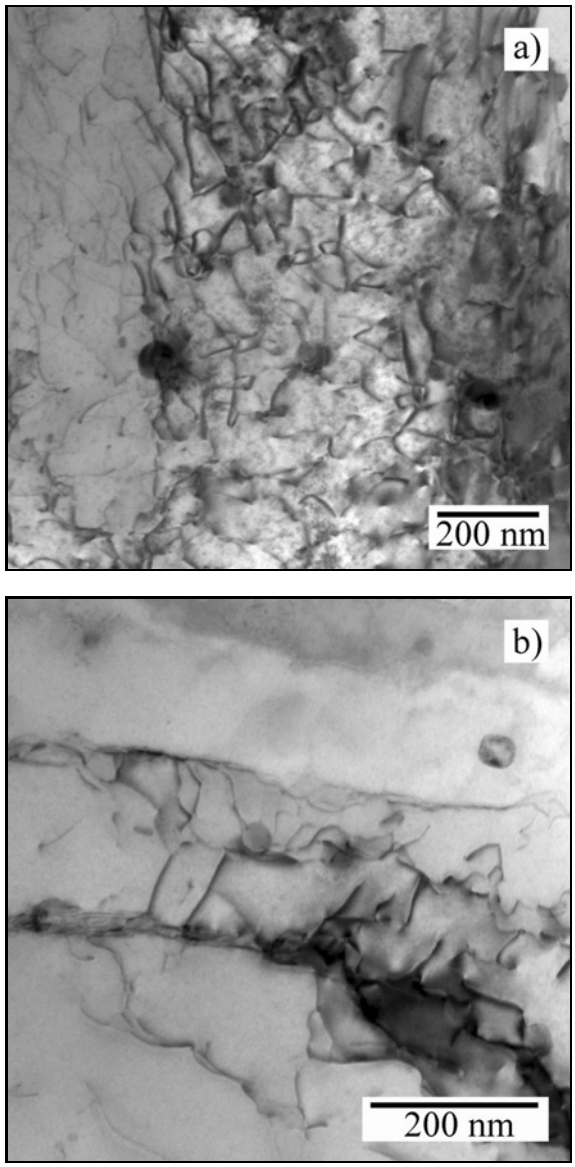

Fig. 5. Bright field TEM micrographs showing the interactions of dislocations with β-Zr precipitates in the PLB regime (creep at 350 °C and 215 MPa): (a) in grain interior and (b) close to grain boundary.

the physical origin of the threshold stress remains incomplete. Zr1%Nb cladding alloys are significantly strengthened by the formation of the incoherent Nb rich β-Zr precipitates [5, 8], which represent effective obstacles to dislocation movement and, therefore, are the main contributor to the origin of the threshold stress during creep (Fig. 4). The precipitates are round with a mean size of ~ 50 nm, and their volume density was estimated to be $\sim 1 \times 10^{20}$ m^{-3}. Consequently, it is important to consider, hereafter, the interactions between dislocations and β-Zr secondary phase precipitations (Fig. 5). However, it should be noted that the interactions of dislocations with fine β-Zr precipitates

could be studied only to a minimal extent, not only because of the small interparticle spacing but also due to the extreme difficulty in observing both dislocations and the particles simultaneously. The coarse minor Laves phase $Zr(Nb,Fe)_2$ with a mean size of ~ 200 nm, frequently creating the coalescence of a few individual Laves phase particles, could not significantly affect the precipitation strengthening.

Several mechanisms have been proposed for the origin of the threshold stress, σ_0. Lund and Nix [27] introduced the idea that the threshold stress could be equated with the Orowan stress, σ_{Or} [13, 16, 17, 27–32]. There are two main mechanisms susceptible for dislocations to escape from the pinning particles: (i) particle cutting and (ii) Orowan bowing between particles [16, 17, 26]. The former mechanism involves coherent particles. Because the Nb rich β-Zr precipitates are incoherent [8, 26] in a Zr1%Nb alloy [8], the Orowan loop mechanism seems to be more acceptable in the present study.

Come back to the question of whether the enormous values of the stress exponent, n, in the region of the highest stresses in Fig. 1a (PLB regime) can be explained by precipitation strengthening from dislocations-precipitation interactions and in this case, creep is driven by effective stress, σ_{e}, but not by applied stress, σ. The alternative of such extremely high values of n is the inherent characteristic of the creep behaviour in the PLB regime. Figure 6 shows the dependence of the minimum creep rate, $\dot{\varepsilon}_{\mathrm{m}}$, on the effective stress, σ_{e}. Mutual comparison of Figs. 1a, 6 indicates no significant change in the values of the stress exponent, n, (Eq. (2)) and the true stress exponent, n^* (Eq. (6)).

3.3. Link between creep deformation and fracture

In several studies, it was observed that zirconium alloys appear to obey the Monkman-Grant relationship [8, 16, 33, 34]. Using the Monkman-Grant phenomenological relationship [35–37], the minimum creep rate, $\dot{\varepsilon}_{\mathrm{m}}$, can be inversely linked to the time to fracture, t_{f} :

$$(\dot{\varepsilon}_{\mathrm{m}})^{\alpha}\, t_{\mathrm{f}} = C_{\mathrm{MG}}. \tag{10}$$

In various metallic materials and under broad creep loading conditions, the exponent α ranges from about 0.8 to 1.0 [16]. Figure 7 depicts in a double logarithmic plot the Monkman-Grant empirical relationship applied to the creep data of a Zr1%Nb alloy exposed to 350 ℃. From Fig. 7, it can be seen that nearly all the experimental data can be fitted with very good confidence by a single line over the whole interval of the applied stress representing the transition from the power-law to power-law breakdown regimes,

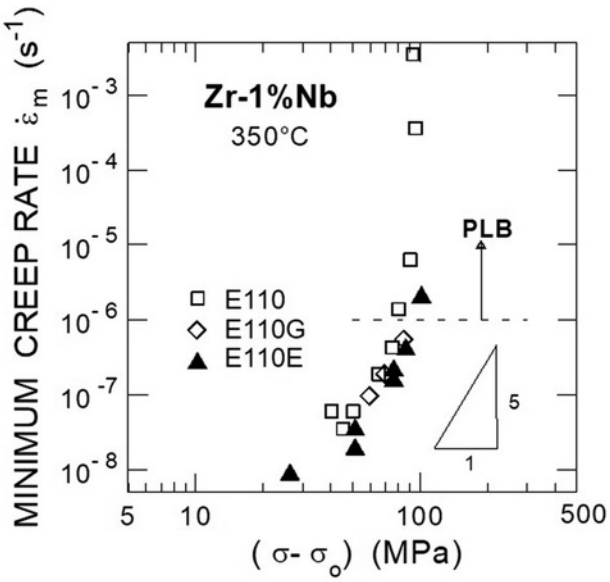

Fig. 6. Dependence of the minimum creep rate, $\dot{\varepsilon}_{\mathrm{m}}$, on the effective stress, σ_{e}.

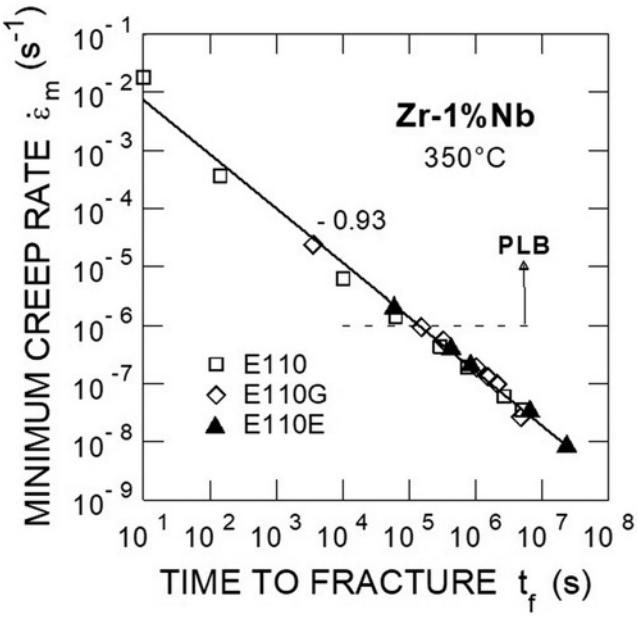

Fig. 7. Dependence of the time to fracture, t_{f}, on the minimum creep rate, $\dot{\varepsilon}_{\mathrm{m}}$ (Monkman-Grant relationship [35]).

and the minimum creep rate, $\dot{\varepsilon}_{\mathrm{m}}$, is inversely linked to the creep life, t_{f}. The fact that the experimental results obey the Monkman-Grant relationship supports two ideas: (i) the mechanisms of creep deformation in both PL and PLB regimes do not change qualitatively, and (ii) the experimental results indicate a close relationship between creep deformation and fracture processes.

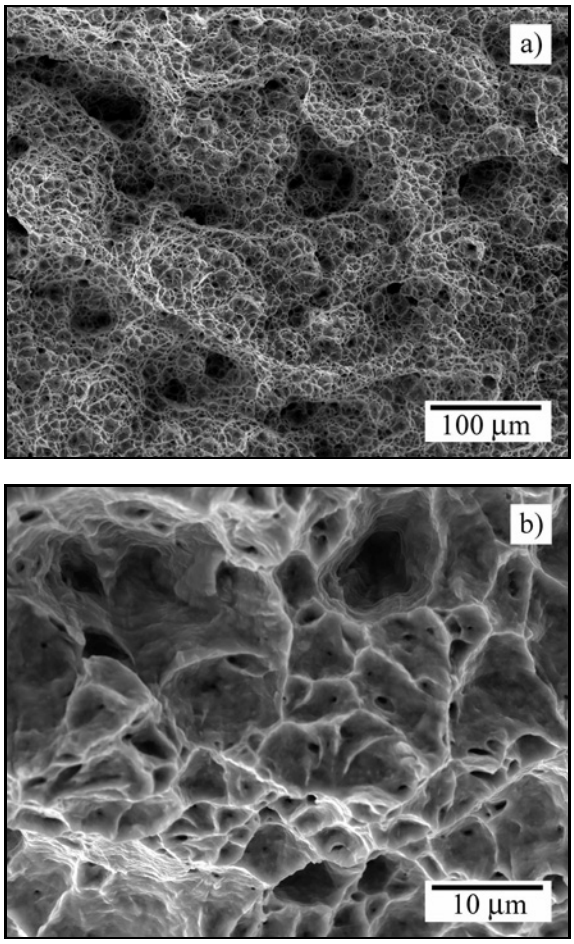

Fig. 8. SEM fractographs of a creep fracture surface of the specimen fractured in the PLB regime (350 °C, 210 MPa, $t_f = 1.8$ h): (a) ductile transgranular mode with creep cavitation and (b) detail of a creep fracture surface.

Fracture surface examination by SEM of the creep fractured specimens from both the PL and PLB regimes did not prove any significant difference. The corresponding SEM fractographs of the creep fracture surfaces taken in the PLB regime are characterized by ductile dimple mode with the presence of extensive creep cavitation coalescence, as shown in Fig. 8. However, a detailed fractographic investigation of the metallographic longitudinal sections of the fractured specimens revealed a different distribution homogeneity of creep cavities along the gauge length and at the cross-section of the fracture specimens tested in the PL and PLB regimes. Whereas creep cavitation at moderate creep stresses was more or less homogeneously distributed in the deformed part of the fractured specimens, at the highest stresses (in the PLB regime), a limited extent of the creep cavities was observed in close proximity to the fracture surface. Supposing the link between deformation and damage processes, this finding may indicate different homogeneity

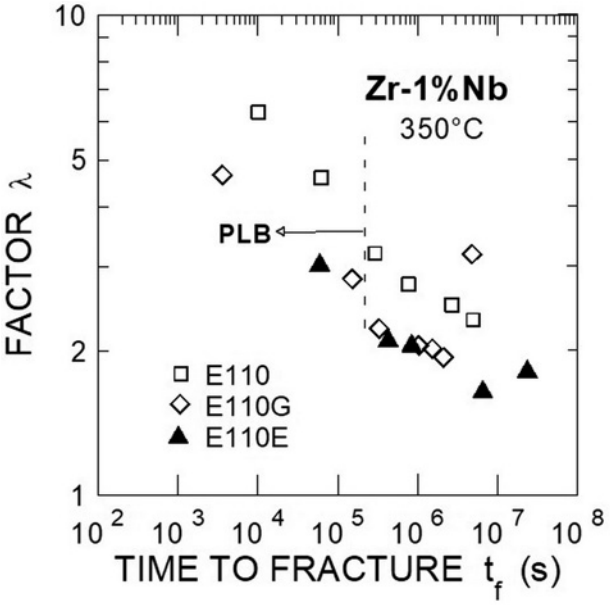

Fig. 9. Plot of the creep damage tolerance factor λ vs the time to fracture t_f.

of acting deformation processes in the PL and PLB regimes. Nevertheless, in both creep regimes, the final creep fracture is due to a local loss of stability of plastic deformation (necking) and exhibits a mixture of the ductile transgranular mode with an inferior synergistic effect of creep intergranular cavitation.

A further basis for comparing the creep damage and fracture in the PL and PLB regimes can be obtained using an approach based on a continuum damage mechanics, namely by using the creep damage tolerance factor λ [36, 38–43]. The creep damage tolerance factor, λ, has been defined as the ratio of strain to fracture, ε_f, to the product of the minimum creep rate, $\dot{\varepsilon}_m$, and the time to fracture, t_f [39]:

$$\lambda = \varepsilon_f / \dot{\varepsilon}_m t_f. \tag{11}$$

The creep damage tolerance factor, λ, will be used to assess the creep damage and fracture in the transition between the PL and PLB regimes. From the definition (Eq. (11)), the factor λ can be directly calculated using the experimental creep data. The double logarithmic plot of the calculated values of λ vs time to fracture t_f is shown in Fig. 9, demonstrating the values of λ in the PL and PLB regimes. The calculated values of λ cover the range from ~ 1.7 to ~ 8, demonstrating the dependence of λ on loading conditions ($t_f = t_f(\sigma, T)$). At a constant testing temperature, there is a clear tendency towards a decrease of λ with increasing time to fracture, t_f, and, logically, with increasing applied stress, σ. It is interesting to correlate the determined values λ with the fractographic analysis (compare Fig. 8) and the theoretical interpre-

tation of the values λ according to Ashby and Dyson [39]. From their analysis, it follows that for $\lambda = 1$, metals and alloys exhibit low creep fracture strain and brittle fracture mode without any local deformation. For λ in the range of 1.5–2.5, they suggested that creep damage is due to the combined effect of power-law and diffusion creep. Larger values of λ indicate microstructural instability, the ductile fracture mode, and the dominant fracture process is necking. Thus, we can conclude that the experimentally evaluated values λ (Fig. 9) based on the creep data reasonably predict the observed creep fracture mode (Fig. 8).

3.4. Rate controlling mechanisms

Considerable attention has been given to the deformation mechanisms operating in power-law creep [16, 17, 44]. The general consensus is that the power-law creep regime is assumed to be diffusion-controlled, and the acting controlling creep deformation mechanism is associated with dislocation climb. This is evident from the equivalence between the experimentally determined activation energy for creep and that for self-diffusion [16]. In the case of zirconium, dislocation climb may be an easier process than dislocation glide because high diffusivity and a low value of the elastic modulus lead to a high climb rate. Furthermore, most models suppose that creep in polycrystalline metals and alloys occurs mainly by homogeneous intragranular deformation. This premise was criticized by Nabarro [44] as irrelevant. However, reliable evidence of whether the mechanisms operating in power-law and power-law breakdown regimes are the same or different is still missing.

Nevertheless, as mentioned earlier, a view on the rate controlling creep mechanism(s) in the PLB regime has not yet been successfully answered. A variety of theories has been reported over the past five decades but has not been sufficiently verified [44–51]. Very recently, Kassner and Ermagan [50] published a new analysis that provides contemporary insight into frequently considered mechanisms of power-law breakdown in the creep of metals. Kassner and Ermagan [50] anticipated that a dramatic supersaturation of vacancies leading to very high diffusion rates and enhanced dislocation climb is associated with the rate-controlling process for creep in the PLB regime. It should be noted that in an earlier work by Sherby and Burke [45], an idea was already propounded that excess lattice vacancies by dislocation intersection processes in creep at high stresses will enhance dislocation climb and, therefore, make creep easier. Mecking and Estrin [52] did not accept the possibility of vacancy supersaturation in the power-law regime but suggested that such a case may occur within the power-law breakdown regime. Recently, some experiments [53-57], mostly on materials processed by severe plastic deformation – SPD (e.g., equal-channel angular pressing [58]), verified excess of vacancies by intensive deformation. Small-angle X-ray scattering on SPD processed aluminium and its alloy carried out by Betekhtin et al. [55] provided insights into the effect of SPD on free volume (an excess of nonequilibrium vacancies), which was interpreted in terms of nanoporosity. Furthermore, it can be expected that due to an increase in dislocations density in the power-law creep regime, the effect of vacancy supersaturation will be synergistically intensified by dislocation short circuit paths. In such a way, profuse vacancy generation during intense plastic deformation may promote nanoporosity and/or creep cavitation [55, 59–64].

From Eq. (1), it follows that the minimum creep rate, $\dot{\varepsilon}_\mathrm{m}$, is a function not only of stress, σ, but also of the testing temperature T. Therefore, creep mechanisms under consideration should also respect the dependence of creep rate on the temperature, which is generally described by the Arrhenius law:

$$\dot{\varepsilon} = \dot{\varepsilon}_0 \exp\left(-Q_\mathrm{c}/kT\right), \tag{12}$$

where $\dot{\varepsilon}_0$ is the frequency factor, Q_c is the activation energy of creep, and k is the Boltzmann's constant. The most frequently used experimental method of determining the activation energy of creep consists of evaluating the minimum creep rate, $\dot{\varepsilon}_\mathrm{m}$, for various applied stresses, σ, using isothermal creep tests. Thus, with respect to Eq. (12), the activation energy of creep, Q_c, can be defined as

$$Q_\mathrm{c} = \left[\partial \ln \dot{\varepsilon}_\mathrm{m} / \partial \left(-1/kT\right)\right]_\sigma \tag{13}$$

and Q_c can be obtained as a k-multiple of the slope of a $\dot{\varepsilon}_\mathrm{m}$ vs $1/T$ plot. There is a general view that Q_c corresponds to that of lattice self-diffusion, Q_sd, in the PL regime [16, 17]. Hayes and Kassner [2] reported that the activation energy for creep, Q_c, for zirconium and its alloys is reasonably consistent with Q_sd below approximately 650 ℃, which may be associated with dislocation climb. This limitation may be caused by a transformation from the α-Zr to the $(\alpha + \beta)$-Zr phase regions [8]. Generally, the reason that the activation energy for creep and operating creep mechanism(s) in the PLB regime remains poorly understood is due to the inconsistent existing theories and very limited number of experimental studies that have been carried out in this regime [2, 6, 7, 16, 17]. However, recently published works [6, 7] suggest the creep deformation mechanism, which could be dislocation climb but enhanced by short circuit diffusion of vacancies through the large dislocation cores generated at high applied stresses. Finally, it cannot be excluded that the power-law and the power-law breakdown regimes must be treated separately. Concerning the fact that our creep tests were carried out at only one testing temperature

in accordance with the aim of the study, no determination of Q_c was performed. Nevertheless, our future experiments will be carried out within the PLB regime at a broader range of testing temperatures.

4. Conclusions

Tensile creep tests under high constant applied stresses ranging from 150 to 260 MPa at a testing temperature of 350 ℃ have been carried out on three different cladding tubes of the Zr1%Nb alloy having slightly different chemical compositions. The above experimental conditions represent the transition between the power-law (PL) and the power-law breakdown (PLB) regimes. The following conclusions can be drawn from the present investigation:

(i) All Zr1%Nb alloys under investigation reach the PLB regime at values of compensated applied stress σ/G above approximately 8×10^{-3}, where the stress exponent of the minimum creep rate, n, then dramatically increases with increasing stress ratio σ/G from the value of ~ 6 up to ~ 65.

(ii) The value $n \sim 6$ determined at the medium applied stresses is usually considered to be associated with the power-law creep in zirconium and its alloys, and the anticipated controlling mechanism is dislocation climb.

(iii) All experimental creep data obtained from the PL and PLB regimes obey the Monkman-Grant relationship, supporting the idea that the creep deformation mechanism in the PL and PLB regimes does not change qualitatively and indicating a close link between deformation and fracture processes in both creep regimes.

Acknowledgements

Financial support for this work was provided by the Technology Agency of the Czech Republic under Grants No. TH02020477 and No. TN01000015 and is gratefully acknowledged. The authors would like to give special thanks to Drs. Věra Vrtílková and Jakub Krejčí of UJP PRAHA a.s., Prague, Czech Republic, for their technical support and very helpful discussion.

References

[1] B. A. Gurovich, A. S. Frolov, E. A. Kuleshova, D. A. Maltsev, D. V. Safronov, E. A. Alekseeva, TEM-studies of dislocation loops and niobium-based precipitates in E110 alloy after operation in VVER-type reactor conditions, Mater. Charact. 150 (2019) 22–30. doi:10.1016/j.matchar.2019.01.014.

[2] T. A. Hayes, M. E. Kassner, Creep of zirconium and zirconium alloys, Metall. Mater. Trans. A 37A (2006) 2389–2396. doi:10.1007/BF02586213

[3] M. Pahutová, J. Čadek, V. Černý, Steady-state creep of Zr-Nb alloys in a temperature interval 350 to 550 °C, J. Nucl. Mater. 61 (1976) 285–296. doi:10.1016/002-3115(76)90267-1

[4] I. Charit, K. L. Murty, Creep behavior of niobium-modified zirconium alloys, J. Nucl. Mater. 374 (2008) 354–363. doi:10.1016/j.jnucmat.2007.08.019

[5] D. Kaddour, A.-F. Gourgues-Lorenzon, J.-Ch Brachet, L. Portier, A. Pineau, Microstructural influence on high temperature creep flow of Zr1%NbO alloy in near α, $(\alpha + \beta)$, and β temperature ranges in a high vacuum environment, J. Nucl. Mater. 408 (2011) 116–124. doi:10:1016/j.jnucmat.2010.11.025

[6] K. L. Murty, S. Gallapudi, K. Ramaswamy, M. D. Mathew, I. Charit, Creep deformation of materials in light water reactors (LWRs), In: K. L. Murty (Ed.) Material's ageing and degradation in light water reactors – Mechanisms and Management, Woodhead Publishing Series in Energy No. 44, Woodhead Publishing Limited, Oxford, UK, 2013, pp. 81-148. doi:110.1533/9780857097453.1.81

[7] M. E. Kassner, R. Ermagan, Power law breakdown in the creep in single-phase metals, Metals 9 (2019) No. 1345. http://doi:org/10.3390/met9121345

[8] V. Sklenicka, P. Kral, K. Kucharova, M. Kvapilova, J. Dvorak, L. Kloc, Thermal creep fracture of a Zr1%Nb cladding alloy in the α and $(\alpha + \beta)$ phase regions, J. Nucl. Mater. 553 (2021) No. 152950. doi:10.1016/j.jnucmat.2021.152.950.

[9] M. E. Kassner, M. T. Perez Prado, T. A. Hayes, L. Jiang, S. R. Barrabes, I. F. Lee, Elevated temperature deformation of Zr to large strain, J. Mater. Sci. 48 (2013) 4492–4500. doi:10.1007/s10853-012-7060-4

[10] F. Garofalo, An empirical relation defining the stress dependence of minimum creep rate in metals, Trans. AIME 227 (1963) 351–355.

[11] R. Lagneborg, B. Bergman, The stress-creep rate behaviour of precipitation-hardened alloys, Metal Sci. 10 (1976) 20–28. doi:10.1179/030634576790431462

[12] J. C. Gibeling, W. D. Nix, The description of elevated temperature deformation in terms of threshold stresses and back stresses: A review, Mater. Sci. Eng. 45 (1980) 123–135. doi:10.1016/0025-5416(80)90218-9

[13] J. C. Gibeling, Interpretation of threshold stresses and obstacle strengths in creep of particle strengthened materials, In: R. S. Mishra, A. M. Mukherjee, K. Linga Murty (Eds.), Creep behavior of advanced materials for the 21st century. The Minerals, Metals & Materials Society,Warrendale, PA, 1999, pp. 239–253. ISBN No. 0-87339-420-8.

[14] C. N. Ahlquist, R. Gasca-Neri, W. D. Nix, A phenomenological theory of steady state creep based on average internal and effective stresses, Acta Metal. 18 (1970) 663–671. doi:10.1016/0001-6160(70)90096-9

[15] I. Saxl, F. Kroupa, Relations between the experimental parameters describing the steady-state and transient creep, Phys. Stat. Sol. (A) 11 (1972) 167–173. doi:10.1002/pssa.2210110118

[16] J. Čadek, Creep in metallic materials, Elsevier Science Publishers, Amsterdam, The Netherlands, 1988. ISBN 0-444-98916-1.

[17] M. E. Kassner, Fundamentals of creep in metals and alloys, Elsevier Ltd., Amsterdam, The Netherlands, Second edition, 2009. ISBN: 978-0-0804-7561-5.

[18] G. B. Gibbs, Creep and stress relaxation studies with polycrystalline magnesium, Philos. Mag. 13 (1966) 317–329. doi:10.1080/14786436608212610
[19] C. N. Ahlquist, W. D. Nix, A technique for measuring mean internal stress during high temperature creep, Scr. Metall. 3 (1969) 679–681. doi:10.1016/0036-9748%2869%2990076-3
[20] M. Pahutová, J. Čadek, Interpretation of high temperature creep in alpha-zirconium in terms of effective stress and dislocation dynamics, Mater. Sci. Eng. 11 (1973) 151–162. doi:10.1016/0025-5416(73)90061-X
[21] F. A. Mohamed, K. T. Park, E. J. Lavrenia, Creep behavior of discontinuous SiC-Al composite, Mater. Sci. Eng. A 150 (1992) 21–35. doi:10.1016/0921-5093(90)90004-M
[22] J. Čadek, H. Oikawa, V. Šustek, Threshold creep behavior of discontinuous aluminium and aluminium alloy matrix composites: An overview, Mater. Sci. Eng. A 190 (1995) 9–23. doi:10.1016/0921-5093(94)09605-V
[23] Y. Li, T. G. Langdon, A simple procedure for estimating threshold stresses in the creep of metal matrix composites, Scripta Mater. 36 (1997) 1457–1460. doi:10.1016/S1359_6462(97)00041-9
[24] Y. Li, V. Sklenicka, T. G. Langdon, Creep properties of an AZ91 magnesium based composite, in: R. S. Mishra, A. K. Mukherjee, K. Linga Murty (Eds.), Creep behavior of advanced materials for the 21st century. The Minerals, Metals & Materials Society, Warrendale, PA, 1999, pp. 171–178. ISBN: 0-87339-420-8.
[25] R. S. Mishra, T. R. Bieler, A. K. Mukherjee, Superplasticity in powder metallurgy aluminium alloys and composites, Acta Mater. 43 (1995) 877–891. doi:10.1016/0956-7151(94)00323-A
[26] K. Guguloth, R. Mitra, S. G. Chowdhury, J. Swaminathan, Mechanism of creep deformation with evolution of microstructure and texture of Zr-2.5Nb alloy, Mater. Sci. Eng. A 721 (2018) 286–302. doi:10.1016/j.msea.2018.02.035 .
[27] R.W. Lund, W. D. Nix, High temperature creep of Ni-20Cr-2ThO_2 single crystals, Acta Metall. 24 (1976) 469–481. doi:10.1016/0001-6160(76)90068-7
[28] L. M. Brown, R. K. Ham, Dislocation-particle interaction, In: A. Kelly, R. B. Nicholson (Eds.) Strengthening methods in crystals. Applied Science Publishers Ltd., Barking, Essex, England, 1971, Chapter 2, pp. 9–135. ISBN-10:0-444-20105-X.
[29] E. Arzt, Creep of dispersion strengthened materials: A critical assessment, Res Mechanica 31 (1991) 339–453. ISSN: 0143-0084.
[30] E. Arzt, G. Dehm, P. Gumbsch, O. Kraft, D. Weiss, Interface controlled plasticity in metals: Dispersion hardening and thin film deformation, Prog. Mater. Sci. 46 (2001) 283–307. doi:10.1016/S0079-6425(00)00015-3
[31] B. Reppich, On the dispersion strengthening mechanisms in ODS materials, Z. Metallkde. 93 (2002) 605–613. doi:10.3139/146.020605
[32] K. Maruyama, Fundamental aspects of creep deformation and deformation mechanism map, In: F. Abe, T.-U. Kern, R. Viswanathan (Eds.), Creep-resistant steels, Woodhead Publishing Ltd., Cambridge, England, 2008, pp. 265–278. ISBN 978-1-84569-178-3.
[33] T. A. Hayes, R. S. Rosen, M. E. Kassner, Creep fracture of zirconium alloys, J. Nucl. Mater. 353 (2006) 109–118. doi:10.1016/j.jnucmat.2006.02.093
[34] V. Sklenicka, J. Dvorak, P. Kral, V. I. Betekhtin, A. G. Kadomtsev, M. V. Narykova, S. V. Dobatkin, K. Kucharova, M. Kvapilova, Influence of a prior pressurization treatment on creep behavior of an ultrafine-grained Zr-2.5%Nb alloy, Mater. Sci. Eng. A 820 (2021) 141570. doi:10.1016/j.msea.2021.141570 .
[35] F. C. Monkman, N. J. Grant, An empirical relationship between rupture life and minimum creep rate in creep-rupture test, Proc. ASTM 56 (1956) 593–620.
[36] V. Sklenička, K. Kuchařová, P. Král, M. Kvapilová, J. Dvořák, Applicability of empirical formulas and fractography for assessment of creep life and creep fracture modes of tempered martensitic 9%Cr steel, Kovove Mater. 55 (2017) 69–80. doi:10.4149/km_2017_2_69
[37] K. Maruyama, N. Seiko, K. Yoshimi, Changes in Monkman-Grant relation among four creep regions of modified 9Cr-1Mo steel, Mater. Sci. Eng. A 749 (2019) 223–234. doi:10.1016/j.msea.2019.02.003
[38] I. N. Goodall, R. D. H. Cockcroft, E. J. Chubb, Approximate description of creep-rupture structures, Int. J. Mech. Sci. 17 (1975) 351–360. doi:10.1016/0030-7403(75)90027-2
[39] M. F. Ashby, B. F. Dyson, Creep damage mechanics and micro-mechanisms, Advances in Fracture Research, Volume 1, S. R. Valuri, D. M. R. Taplin, P. Rama Rao, J. F. Knott, R. Dubey, Oxford Pergamon Press, 1984, pp. 3–33.
[40] B. F. Dyson, T. B. Gibbons, Tertiary creep in nickel-base superalloys: Analysis of experimental data and theoretical synthesis, Acta Mater. 36 (1987) 2355–2369. doi:10:1016/0001-6160(87)90083-6
[41] B. Wilshire, H. Burt, Creep strain analysis for steel, In: F. Abe, T-U Kern, R. Viswanathan (Eds.), Creep-resistant steels, Woodhead Publishing Ltd., Cambridge, England, 2008, pp. 421–445. ISBN 978-1-84569-178-3.
[42] B. K. Chaudhari, Tertiary creep behavior of 9Cr-Mo ferritic steel, Mater. Sci. Eng. A 585 (2013) 1–9. doi:10.1016/j.msea.2013.07.026
[43] T. Shresta, M. Basirat, I. Charit, G. P. Potirniche, K. K. Rink, Creep rupture behavior of Grade 91 steel, Mater. Sci. Eng. A 565 (2013) 382–391. doi:10.1016/j.msea.2012.12.031
[44] F. R. N. Nabarro, Do we have an acceptable model of power-law creep? Mater. Sci. Eng. A 387–389 (2004) 659–664. doi:10.1016/j.msea.2003.09.118
[45] O. D. Sherby, P. M. Burke, Mechanical behavior of crystalline solids at elevated temperatures, Prog. Mater. Sci. 13 (1968) 323–390. doi:10.1016/0079-6425(68)90024-8
[46] S. L. Robinson, O. D. Sherby, Mechanical behavior of polycrystalline tungsten at elevated temperature, Acta Metall. 17 (1969) 109–125. doi:10.1016/0001-6160(69)90132-1
[47] H. Luth, A. K. Miller, O. D. Sherby, The stress and temperature dependence of steady-state flow at intermediate temperatures for pure polycrystalline aluminum, Acta Metall. 28 (1980) 169–178. doi:10.1016/0001-6160(80)90066-8
[48] G. M. Pharr, Some observations on the relation between dislocation substructure and power law breakdown in creep, Scripta Metall. 15 (1981) 713–717. doi:10.1016/0036-9748(81)90005-3
[49] P. Yavari, T. G. Langdon, An examination of the breakdown in creep by viscous glide in solid solution

alloys at high stress levels, Acta Metall. 30 (1982) 2181–2189. doi:10.1016/0001-6160(82)90139-0
[50] M. E. Kassner, R. Ermagan, Power-law breakdown in the creep in single-phase metals, Metals 9 (2019) 1345. doi:10.3390/met9121345
[51] W. J. Kim, H. T. Jeong, Easy construction of processing maps for metallic alloys using a flow instability criterion based on power-law breakdown, J. Mater. Res. Technol. 9 (2020) 5134–5143. doi:10.1016/j.jmrt.2020.03.030.
[52] H. Mecking, Y. Estrin, The effect of vacancy generation on plastic deformation, Scr. Metall. 14 (1980) 815–819. doi:10.1016/0036-9748(80)90295-1
[53] J. Cizek, I. Prochazka, R. Kuzel, Z. Matej, V. Cheraska, M. Cieslar, B. Smola, I. Stulikova, G. Bauer, W. Anwand, R. K. Islamgaliev, O. Kulyasova, Ultrafine-grained metals prepared by severe plastic deformation: A positron annihilation study, Acta Physica Pol. A 107 (2005) 747–752. doi:10.12693%2FAPhysPolA.107.745
[54] M. J. Zehetbauer, G. Steiner, E. Schafler, A. Korznikov, E. Korznikova, Deformation induced vacancies with severe plastic deformation: Measurement and modeling, Mater. Sci. Forum 503/504 (2006) 57–64. doi:10.4028/www.scientific.net/MSF.503-504.57
[55] V. I. Betekhtin, A. G. Kadomtsev, V. Sklenicka, I. Saxl, Nanoporosity of fine-crystalline aluminum and an aluminum-based alloy, Phys. Solid State 49 (2007) 1874–1877. doi:10.1134/S1063783407100101
[56] E. Schafler, G. Steiner, E. Korznikova, M. Kerber, M. J. Zehetbauer, Lattice defect investigation of ECAP-Cu by means of X-ray line profile analysis, calorimetry and resistometry, Mater. Sci. Eng. A 410–411 (2005) 169–173. doi:10.1016/j.msea.2005.08.070
[57] S. V. Divinski, G. Reglitz, H. Rösner, Y. Estrin, G. Wilde, Ultra-fast diffusion channels in pure Ni severely deformed by equal-channel angular pressing, Acta Mater. 59 (2011) 1974–1985. doi:10.1016/j.actamat.2010.10.005
[58] R. Z. Valiev, R. K. Islamgaliev, I. V. Alexandrov, Bulk nanostructured materials from severe plastic deformation, Prog. Mater. Sci. 45 (2000) 10–189. doi:10.1016/S0079-6425(99)00007-9
[59] R. Lapovok, D. Tomus, J. Mang, Y. Estrin, T. C. Lowe, Evolution of nanoscale porosity during equal-channel angular pressing of titanium, Acta Mater. 57 (2009) 2909–2918. doi:10.1016/j.actamat.2009.02.042
[60] V. I. Betekhtin, V. Sklenicka, I. Saxl, B. K. Kardashev, A. G. Kadomtsev, M. V. Narykova, Influence of the number of passes under equal-channel angular pressing on the elastic-plastic properties, durability, and defect structure of the Al + 0.2wt.%Sc, Phys. Solid State 52 (2010) 1629–1636. doi:10.1134/S1063783410080111
[61] I. A. Ovidko, A. G. Sheinerman, N. V. Skiba, Elongated nanoscale voids at deformed special grain boundary structures in nanocrystalline materials, Acta Mater. 59 (2011) 678–685. doi:10.1016/j.actamat.2010.10.005
[62] J. Dvorak, V. Sklenicka, V. I. Betekhtin, A. G. Kadomtsev, P. Kral, M. Kvapilova, M. Svoboda, The effect of hydrostatic pressure on creep behavior of pure Al and a Cu-0.2wt.%Zr alloy processed by equal-channel angular pressing, Mater. Sci. Eng. A 584 (2015) 103–113. doi:10.1016/j.msea.2013.07.018
[63] A. V. Weckman, B. F. Dem'yanov, Simulation of the pore formation at grain boundaries in aluminum, JETP Letters 111 (2020) 643–646. doi:10.1134/s0021364020110119
[64] V. I. Betekhtin, A. G. Kadomtsev, M. V. Narykova, Evolution of a defect structure during creep tests of ultrafine-grained metals and alloys produced by severe plastic deformation, Phys. Solid State 62 (2020) 318–324. doi:10.1134/S1063783420020067